Chapter 6
Planning for Freeform Surface Measurement

In this chapter, we present a sensing strategy for determining the probing points for achieving efficient measurement and reconstruction of freeform surfaces. B-spline is adopted for modeling the freeform surface. In the framework of Bayesian statistics, we develop a model selection strategy to obtain an optimal model structure for the freeform surface. Based on the selected model structure, a set of probing points are then determined where measurements are to be taken. In order to obtain reliable parameter estimation for the B-spline model, we analyze the uncertainty of the model and use the statistical analysis of the Fisher information matrix to optimize the locations of the probing points needed in the measurements. Using a "data cloud" of a surface acquired by a 3D vision system, we implemented the proposed method for reconstructing freeform surfaces. The experimental results show that the method is effective and promises useful applications in multi-sensor measurements including vision-guided CMM for reverse engineering.

6.1 The Problem

Reconstructing the freeform surface from a set of discrete measurement data points is a problem important to many areas including reverse engineering, metrology, inspection by machine vision, computer-aided design (Song and Kim 1997, Thompson and Owen 1999, Wolovich et al. 2002, Weir et al. 2000). The first task in the reconstruction of a freeform surface is to obtain the measurement data. Among the various sensing techniques available, mechanical contact probes such as CMM (Coordinate Measuring Machine)'s touch probe, and 3D topography measuring systems using structured light or fringe illumination are widely used in practical applications. CMM with touch-triggered probes can provide high measurement accuracy at sub-micron level. However, the measurement speed is much lower than that of a 3D vision system. A vision system can acquire thousands of data points over a large spatial range in a snapshot (Li and Chen 2003). However, the achievable resolution is relatively low, at around 100–200 μm. Therefore, in practical applications, using one of the techniques means that the user has to suffer from its limitations, e.g. the low speed with CMM.

A way to overcome the limitations of individual sensing techniques lies in integrating multiple sensors in the measurement as conceptualized in Fig. 6.1. Research efforts have been made to achieve this. For example, Nashman et al.

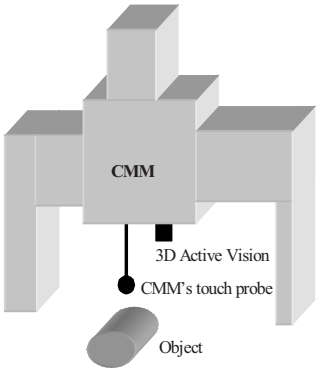

Fig. 6.1. Multiple-sensor coordinate measuring system

(1996) integrated vision in a touch-probe system, where a video camera with a laser triangulation probe and a 3D touch probe were used in a CMM. They presented a cooperative interaction method for the vision and touch-probe system that provided sensory feedback to the CMM for dimension inspection tasks. Chen and Lin (1997) presented a vision-aided reverse engineering approach (VAREA) to reconstruct free-form surface models from physical models, with a CMM equipped with a touch-triggered probe and a vision system. The VAREA integrated computer vision, surface data digitization and surface modeling into a single process. The initial vision-driven surface triangulation process (IVSTP) generated a triangular patch by using stereo image detection and a constrained Delaunay triangulation method. The adaptive model-based digitization process then refined the surface reconstruction using measurements from the CMM's touch probe. Since the vision system in VAREA used a 3D stereo algorithm to detect 3D surface boundaries, only 3D surface boundaries were reconstructed and geometrical information about the freeform surface could not be retrieved. Recently, Shen et al. (2000, 2001) presented a multiple-sensor coordinate measuring system for automated part localization and rapid surface digitization. The multiple-sensor system consists of a high-precision CMM equipped with a touch probe and a 3D active vision system. Their research focused on setting up a multiple-sensor system and processing the geometrical information from the vision system. In these systems, the CMM's touch probe plays the role of accurately digitizing a surface, especially when high-precision is desired. The question of how to determine the set of measurement data, including the needed number of the measurement data points and their locations, for accurate reconstruction of freeform surfaces, remains untouched.

Using a CMM for 3D measurements, only a finite number of discrete measurement data can be taken for a surface. From the statistical viewpoint, each measurement data point contains a certain amount of geometrical information about the surface, and the quantity of information contained in the set of measurement data points depends on the number and locations of the measurement points.

Considering the lengthy time needed in using a CMM to take a large number of measurement data points, we should select the locations of the data points to achieve an optimal measurement and reconstruction. Unfortunately, the current practice in using CMM mostly adopts random data point setting on a surface. In such a case, each data point has an equal probability of being picked for the measurement. For example, Woo et al. (1995) presented a sampling strategy based on Hammersley sequence to determine the number of discrete sample points and their locations on a machined surface (Woo and Liang 1993). Lee et al. (1997) proposed a feature-based method, which integrates Hammersley sequence and a stratified sampling method, to derive the sampling strategy for various surfaces such as circular, conic, cylindrical, rectangular and spherical surfaces.

Unlike objects composed of simple geometric primitives, such as planes, lines, spheres and cylinders, freeform surfaces have no obvious features. Therefore, they are more difficult to define and model mathematically than simple geometric objects. In most cases, freeform surfaces are represented by the parametric equations such as Coons patches (Farin 2002), B-splines, or NURBS (non-uniform rational B-splines). A fundamental question then arises: can we find the parametric model to represent an unknown freeform surface and then select a minimal set of discrete measurement points to obtain these parameters, while controlling the uncertainty of model parameters within a specified tolerance. Here, the uncertainty describes the tolerance range within which the unknown true surface lies with some confidence levels. The lower the uncertainty of the model, the better the reconstructed surface is. In this chapter, we propose a method that allows for optimal measurements and reconstruction of freeform surfaces. Two issues need to be addressed here. The first is how to select the model structure using a cloud of low-precision data acquired by a 3D vision sensor. We use B-splines to represent a freeform surface and present a Modified BIC (Bayesian Information Criterion) approach for selecting an optimal model structure for surface representation. The second is how to determine the locations of a set of measurement data points for high-precision measurements e.g. by CMM's touch probe. In our work, we analyze the uncertainty of the B-spline model and use the statistical analysis of the Fisher information matrix (Wang 1999) which measures the uncertainty of the parameters of the model, to optimize the locations of the measurement data points to minimize the uncertainty of the model.

The rest of this chapter is organized as follows. Section 6.2 describes the B-splines approximation and model selection for the 3D reconstruction of freeform surface. In Sect. 6.3, the uncertainty of the B-spline surface is analyzed. Section 6.4 presents the optimization of the locations of measurement data points. Section 6.5 gives some experimental results in reconstructing the freeform surfaces of some real objects. Finally, conclusions of the work are given in Sect. 6.6.

6.2 B-Spline Model Representation

6.2.1 B-Spline Representation

A B-spline surface is defined by the following equation

$$s(u,v) = \sum_{i=0}^{n_u-1} \sum_{j=0}^{n_v-1} B_{i,p}(u) \cdot B_{j,q}(v) \cdot \phi_{ij} . \tag{6.1}$$

where n_u and n_v are the number of control points in u and v directions; ϕ_{ij} ($i = 0,1,\ldots,n_u-1$, $j = 0,1,\ldots,n_v-1$) are the n ($n = n_u \times n_v$) control points; $B_{i,p}(u)$ and $B_{j,q}(v)$ are the normalized B-splines of degree p and q for the u and v directions respectively which are defined over the knot vectors $\mathbf{u} = [u_0, u_1, \ldots, u_{n_u+p}]$ and $\mathbf{v} = [v_0, v_1, \ldots, v_{n_v+q}]$.

Assume that (x_k, y_k, z_k) are the coordinates of a measurement point $\mathbf{r}_k$ on the surface, with location parameters (u_k, v_k). Let us further assume that the degrees of p and q and the complete knot vectors **u** and **v** for surface fitting are also determined. By introducing the measurement point $\mathbf{r}_k$ with the corresponding location parameters [u_k, v_k] in (6.1), we have

$$\begin{cases} x_k = \sum_{i=0}^{n_u-1} \sum_{j=0}^{n_v-1} B_{i,p}(u_k) B_{j,q}(v_k)\, x_{ij} \\ y_k = \sum_{i=0}^{n_u-1} \sum_{j=0}^{n_v-1} B_{i,p}(u_k) B_{j,q}(v_k)\, y_{ij} \\ z_k = \sum_{i=0}^{n_u-1} \sum_{j=0}^{n_v-1} B_{i,p}(u_k) B_{j,q}(v_k)\, z_{ij} \end{cases} \tag{6.2}$$

where (x_{ij}, y_{ij}, z_{ij}) are the coordinates of the B-spline surface control points ϕ_{ij}. (6.2) can be expressed as a linear combination of the control points in the B-spline representation,

$$\begin{cases} x_k = \mathbf{B}_k \cdot \mathbf{\Phi}_x \\ y_k = \mathbf{B}_k \cdot \mathbf{\Phi}_y \\ z_k = \mathbf{B}_k \cdot \mathbf{\Phi}_z \end{cases} \tag{6.3}$$

where

$$\mathbf{B}_k = [[(B_{i,p}(u_k) \cdot B_{j,q}(v_k))_{j=0}^{n_v-1}]_{i=0}^{n_u-1}] = [\overline{B}_{k,0}, \overline{B}_{k,1}, \ldots, \overline{B}_{k,n-1}]$$

and

$$\mathbf{\Phi}_x = [[(x_{ij})_{j=0}^{n_v-1}]_{i=0}^{n_u-1}]^T,$$
$$\mathbf{\Phi}_y = [[(y_{ij})_{j=0}^{n_v-1}]_{i=0}^{n_u-1}]^T,$$
$$\mathbf{\Phi}_z = [[(z_{ij})_{j=0}^{n_v-1}]_{i=0}^{n_u-1}]^T.$$

If a total of *m* points on the surface are considered, we have

$$\begin{cases} \mathbf{x} = \mathbf{B} \cdot \mathbf{\Phi}_x \\ \mathbf{y} = \mathbf{B} \cdot \mathbf{\Phi}_y \\ \mathbf{z} = \mathbf{B} \cdot \mathbf{\Phi}_z \end{cases}, \tag{6.4}$$

where $\mathbf{x} = [x_1, x_2, \ldots, x_m]^T$, $\mathbf{y} = [y_1, y_2, \ldots, y_m]^T$ and $\mathbf{z} = [z_1, z_2, \ldots, z_m]^T$. $\mathbf{B}$ is a matrix consisting of the tensor products of the B-spline basis functions corresponding to each of the *m* measurement points on the surface:

$$\mathbf{B} = \begin{bmatrix} \overline{B}_{0,0} & \overline{B}_{0,1} & \cdots & \overline{B}_{0,n-1} \\ \overline{B}_{1,0} & \overline{B}_{1,1} & \cdots & \overline{B}_{1,n-1} \\ \vdots & \vdots & \cdots & \vdots \\ \overline{B}_{m-1,0} & \overline{B}_{m-1,1} & \cdots & \overline{B}_{m-1,n-1} \end{bmatrix}.$$

If $\mathbf{B}$ in (6.4) is of full rank, then $\mathbf{B^T B}$ is nonsingular. The least square estimation of $\mathbf{\Phi} = [\mathbf{\Phi}_x^T, \mathbf{\Phi}_y^T, \mathbf{\Phi}_z^T]^T$ can be given as:

$$\begin{cases} \mathbf{\Phi}_x = [\mathbf{B^T B}]^{-1} \mathbf{B^T} \cdot \mathbf{x} \\ \mathbf{\Phi}_y = [\mathbf{B^T B}]^{-1} \mathbf{B^T} \cdot \mathbf{y} \\ \mathbf{\Phi}_z = [\mathbf{B^T B}]^{-1} \mathbf{B^T} \cdot \mathbf{z} \end{cases} \tag{6.5}$$

where $[\mathbf{B^T B}]^{-1} \mathbf{B^T}$ is the pseudo-inverse matrix of $\mathbf{B}$.

6.2.2 Model Selection

It is known that for a given set of measurement data, there exists a model of optimal complexity that has the smallest prediction/generalization errors for further data. For a B-spline surface, the model complexity is related to the number n ($n = n_u \times n_v$) of control points (parameters) in the u and v directions in the parameter field (Yan et al. 1999). If the B-spline model contains too many control points, the approximated B-spline surface will tend to over-fit noisy measurement data. If the model does not have enough control points, then it will not be able to fit

the measurement data, causing the approximation to be under-fitted. In general, both over- and under-fitted approximation will have a poor generalization capability. Therefore, the problem of finding an appropriate model, referred to as model selection, is important for achieving a high level of generalization capability. The problem of model selection has been studied from various standpoints. Examples include information statistics (Sugiyama and Ogawa 2001), Bayesian statistics (Shwartz 1978, Torr 2002) and structural risk minimization (Cherkassky et al. 1999). The Bayesian approach is perhaps the most general and powerful method.

Given a set of models $\{M_k, k = 1,2,\ldots,k_{\max}\}$ and data $\mathbf{r}$, the Bayesian approach selects the model with the largest posterior probability. The posterior probability of model M_k is

$$p(M_k \mid \mathbf{r}) = \frac{p(\mathbf{r} \mid M_k)p(M_k)}{\sum_{L=1}^{k_{\max}} p(\mathbf{r} \mid M_L)p(M_L)} \propto p(M_k \mid \mathbf{r}) \tag{6.6}$$

where $p(\mathbf{r} \mid M_k)$ is the likelihood function of model M_k and $p(M_k)$ is the prior probability of model M_k.

If we assume that the models have the same likelihood a priori, that is $p(M_k) = 1/k_{\max}$, $(k = 1,\ldots,k_{\max})$, the posterior probability $p(M_k \mid \mathbf{r})$ will not be affected by $p(M_k)$. This is also the case with $\sum_{L=1}^{k_{\max}} p(r \mid M_L)p(M_L)$ since it is not a function of M_k. Therefore, the posterior probability $p(M_k \mid \mathbf{r})$ is proportional to $p(\mathbf{r} \mid M_k)$.

To find the model with the largest posterior probability, that is $M = \arg \max_{M_k, k=1,\ldots,k_{\max}} p(M_k \mid \mathbf{r})$, we can evaluate the likelihood function $p(\mathbf{r} \mid M_k)$ of model M_k,

$$M = \arg \max_{M_k, k=1,\ldots k_{\max}} \{p(\mathbf{r} \mid M_k)\} \tag{6.7}$$

To calculate $p(\mathbf{r} \mid M_k)$, we need to calculate multidimensional integration (Torr 2002)

$$p(\mathbf{r} \mid M_k) = \int_{\mathbf{\Phi}_k} p(\mathbf{r} \mid \mathbf{\Phi}_k, M_k)p(\mathbf{\Phi}_k \mid M_k)d\mathbf{\Phi}_k$$

In most practical cases, calculating the multidimensional integration is hard, especially to obtain a closed form analytical solution. The research in this area has resulted in many approximation methods for achieving this. Schwarz (1978) and Torr (2002) used Laplace's approximation method for the integration, and simplified $p(\mathbf{r} \mid M_k)$ to

$$\log p(\mathbf{r} \mid M_k) = \log p(\mathbf{r} \mid \hat{\mathbf{\Phi}}_k, M_k) - \frac{1}{2}\log \mid H(\hat{\mathbf{\Phi}}_k) \mid$$

where $\hat{\mathbf{\Phi}}_k$ is the maximum likelihood estimate of $\mathbf{\Phi}_k$, and $H(\hat{\mathbf{\Phi}}_k)$ is the Hessian matrix of $-\log p(\mathbf{r}\,|\,\mathbf{\Phi}_k, M_k)$ evaluated at $\hat{\mathbf{\Phi}}_k$,

$$H(\hat{\mathbf{\Phi}}_k) = -\frac{\partial^2 \log\, p(\mathbf{r}|\mathbf{\Phi}_k,\, M_k)}{\partial \mathbf{\Phi}_k \partial \mathbf{\Phi}_k^T}\bigg|_{\mathbf{\Phi}_k=\hat{\mathbf{\Phi}}_k}.$$

By approximating $\left(1/2\right)\log|H(\hat{\mathbf{\Phi}}_k)|$ by the asymptotic expected value $\frac{3\log(m)}{2}d_k$ of Hessian, we can obtain the Bayesian Information Criterion (BIC) (Torr 2002) for selecting the structure of the B-spline surface

$$M = \arg \max_{M_k, k=1,..k_{\max}} \left\{ \log p(\mathbf{r}\,|\,\hat{\mathbf{\Phi}}_k, M_k) - \frac{3\log(m)}{2}\cdot d_k \right\} \tag{6.8}$$

where d_k is the number of control points for B-spline model M_k.

Consider the likelihood function of the parameter of the B-spline model. The probability distribution function $p(\mathbf{r}\,|\,\hat{\mathbf{\Phi}}_k, M_k)$ of the surface can be factorized into x, y, and z components as

$$p(\mathbf{r}\,|\,\hat{\mathbf{\Phi}}_k, M_k) = p(x\,|\,\hat{\mathbf{\Phi}}_{kx}, M_k)\cdot p(y\,|\,\hat{\mathbf{\Phi}}_{ky}, M_k)\cdot p(z\,|\,\hat{\mathbf{\Phi}}_{kz}, M_k)$$

Consider the x component. Assuming that the residual error sequence e_{ix} ($e_{ix} = x_i - \mathbf{B}_i\mathbf{\Phi}_{kx}$, i=0,1,…, m–1) obeys Gaussion distribution with zero mean and variance σ_{kx}^2, the $p(x\,|\,\hat{\mathbf{\Phi}}_{kx}, M_k)$ can be calculated by

$$p(\mathbf{x}\,|\,\hat{\mathbf{\Phi}}_{kx}, M_k) = \left(\frac{1}{2\pi\sigma_{kx}^2(\hat{\mathbf{\Phi}}_{kx})}\right)^{m/2} \exp\left\{-\frac{1}{2\sigma_{kx}^2(\hat{\mathbf{\Phi}}_{kx})}\sum_{i=0}^{m-1}[x_i - \mathbf{B}_i\hat{\mathbf{\Phi}}_{kx}]^2\right\} \tag{6.9}$$

with $\sigma_{kx}^2(\hat{\mathbf{\Phi}}_{kx}, M_k)$ estimated by

$$\hat{\sigma}_{kx}^2(\hat{\mathbf{\Phi}}_{kx}) = \frac{1}{m}\sum_{i=0}^{m-1}[x_i - \mathbf{B}_i\hat{\mathbf{\Phi}}_{kx}]^2 \tag{6.10}$$

The $p(y\,|\,\hat{\mathbf{\Phi}}_{kx}, M_k)$ and $p(z\,|\,\hat{\mathbf{\Phi}}_{kx}, M_k)$ for y and z components can also be obtained in the similar way. Therefore, we can obtain the following BIC criterion for selecting a B-splines model

$$M = \arg \max_{M_k, k=1,\ldots k_{\max}} \left\{ -\frac{m}{2} \sum_{f=x,y,z} \log \hat{\sigma}_{kf}^2 (\hat{\boldsymbol{\Phi}}_{kf}) - \frac{3 \cdot \log(m)}{2} \cdot d_k \right\} \tag{6.11}$$

where m is the number of data points. As the first two terms in (6.11) measure the prediction accuracy of the B-spline model, the BIC criterion will increase as the complexity of the model increases. In contrast, the second term will decrease and act as a penalty for using additional parameters to model the data. However, since the predicted $\hat{\sigma}_{kf}^2$ (f=x, y, z) depends only on the training data sampled for model estimation, they are insensitive when under-fitting or over-fitting occurs. In (6.11), only the second term prevents the occurrence of over-fitting. In fact, an honest estimate of σ_{kf}^2 (f=x, y, z) should be based on a re-sampling procedure. Here, we can divide the available data into a training sample and a prediction sample. The training sample is used only for model estimation, whereas the prediction sample is used only for estimating the prediction data noise σ_{kf}^2 (f=x, y, z). That is, the training sample is used to estimate the model parameter $\hat{\boldsymbol{\Phi}}_k$ by (6.5), while the prediction sample is used to predict data noise σ_{kf}^2 (f=x, y, z) by (6.10). In fact, if the model $\hat{\boldsymbol{\Phi}}_k$ fitted to the training data is valid, then the estimated variance $\hat{\sigma}_{kf}^2$ (f=x,y,z) from the prediction sample should also be a valid estimate of the data noise. If the variance $\hat{\sigma}_{kf}^2$ (f=x, y, z) found from the prediction sample becomes unexpectedly large, we have grounds for believing that the candidate model fits the data badly. It is seen that the data noise $\hat{\sigma}_{kf}^2$ (f=x, y, z) estimated from the prediction sample is more sensitive to the quality of the model than the one directly estimated from the training sample, as the $\hat{\sigma}_{kf}^2$ (f=x, y, z) estimated from the prediction sample also has the capability of detecting the occurrence of under-fitting or over-fitting.

6.3 Uncertainty Analysis

Equation (6.5) produces the parameter estimation of a B-spline model. It should be noted that measurement data are normally contaminated by noise, and it is impossible to find an exact solution for the B-spline model. From here on in this section, we will ignore the k in $\hat{\boldsymbol{\Phi}}_{kf}$ (f=x, y, z) and other symbols related to the selected model M_k for simplification. Since the residual sequence e_f (f=x, y, z) obeys Gaussion distribution with zero mean and variance σ_f^2, and the B-spline

model in (6.4) is linear, the parameter errors $\mathbf{\Phi}_f - \hat{\mathbf{\Phi}}_f$ are also a Gaussian distribution with zero mean and covariance

$$\mathbf{C} = \sigma^2 \begin{bmatrix} (\mathbf{B}^{\mathbf{T}}\mathbf{B}) & \mathbf{0} & \mathbf{0} \\ \mathbf{0} & (\mathbf{B}^{\mathbf{T}}\mathbf{B}) & \mathbf{0} \\ \mathbf{0} & \mathbf{0} & (\mathbf{B}^{\mathbf{T}}\mathbf{B}) \end{bmatrix}^{-1} = \sigma^2 \mathbf{M}^{-1}$$

where $\sigma^2 = \sigma_f^2$ (f=x, y, z), which is based on the assumption that the residual sequence e_f (f=x, y, z) has the same covariance. Denoting $\mathbf{\Phi} = [\mathbf{\Phi}_x^T, \mathbf{\Phi}_y^T, \mathbf{\Phi}_z^T]^T$, we consider the following quadratic form

$$(\mathbf{\Phi} - \hat{\mathbf{\Phi}})^{\mathbf{T}} \mathbf{C}^{-1} (\mathbf{\Phi} - \hat{\mathbf{\Phi}}) = \frac{1}{\sigma^2} (\mathbf{\Phi} - \hat{\mathbf{\Phi}})^{\mathbf{T}} \mathbf{M} (\mathbf{\Phi} - \hat{\mathbf{\Phi}})$$

that defines the shape of the Gaussian distribution of the parameter error. In fact, the quadratic form defines a hyper-ellipsoid on which the true model parameters must lie. We do not know the position of the shape as we do not know the true value of $\mathbf{\Phi}$. However, we know the range within which the unknown true $\mathbf{\Phi}$ value lies with a confidence interval. For a confidence level γ, we can find from the distribution a number χ_γ^2 for which there is a probability for γ so that $\frac{1}{\sigma^2}(\mathbf{\Phi} - \hat{\mathbf{\Phi}})^{\mathbf{T}} \mathbf{M} (\mathbf{\Phi} - \hat{\mathbf{\Phi}}) < \chi_\gamma^2$. It follows that there is also a probability for γ that yields the hyper-ellipsoid

$$(\mathbf{\Phi} - \hat{\mathbf{\Phi}})^{\mathbf{T}} \mathbf{M} (\mathbf{\Phi} - \hat{\mathbf{\Phi}}) = \sigma^2 \chi_\gamma^2 \tag{6.12}$$

The true model will be contained in the above ellipsoid which is referred to as the ellipsoid of confidence. The ellipsoid of confidence gives us a useful visual image of the uncertainty of parameter $\mathbf{\Phi}$ of the B-spline surface. In (6.12), $\mathbf{M}$ is also known as the Fisher information matrix (Wang 1999) which characterizes the uncertainty in the estimated parameters. Therefore, the problem of selecting an optimal set of measurement data for CMM's high-precision measurement is to find the locations of the measurement data points for which the estimation uncertainty is minimized in some sense. Various criteria exist for optimizing the Fisher information matrix to achieve minimum estimation errors. The major criterions include *Cond*($\mathbf{M}$), *Trace*($\mathbf{M}$) (A-optimality), the maximum eigenvalue of $\mathbf{M}^{-1}$ (E-optimality), and $|\mathbf{M}|$ (D-optimality) (Wang 1999, Chio and Kurfess 1995). These criteria measure the amount of information contained in the probability distribution representing the parameter errors. Thus, ensuring that the important information and necessary information in the B-spline model is embodied in the measurement data set is the primary concern in selecting an optimal set of measurement data for CMM's high-precision measurement. Here the optimal criterion adopted is the D-optimality, or the determinant criterion, for which the determinant of the Fisher

information matrix |**M**| is to be maximized. Geometrically, the volume of the ellipsoid is inversely proportional to the square root of the determinant |**M**|. A large |**M**| corresponds to a small volume of the model parameter space, indicating that the true parameters are well localized and that the knowledge or information we have about them is highly reliable (Wang 1999, Chio 1995, Whaite 1997). Here, we define |**M**| as the uncertainty measurement for the estimated parameter vector **Φ**.

6.4 Sensing Strategy for Optimizing Measurement

As the uncertainty of a B-spline model is dependent on the number and locations as well as the variance of the measurement data, the sensing strategy plays a critical role in the measurement and reconstruction results. A sensing strategy should be able to determine the number of measurement data to sample and the locations to take the measurements, while keeping the uncertainty of the reconstructed B-spline model sufficiently low.

6.4.1 Determining the Number of Measurement Data

Since the reconstruction of a freeform surface is based on the measurements at discrete points to be sensed by a CMM's touch probe, these discrete points must contain sufficient information that allows the freeform surface to be reconstructed. However, the number of measurement data has to be limited to achieve a reasonable speed in the measurement process. From the statistical point of view, the number of measurement data should be at least ten times the number of the parameters in the B-spline model to make the B-spline regression analysis statistically meaningful (Yang and Menq 1993). For example, for a bi-cubic B-spline surface with d ($d = n_u \times n_v$) control points, at least $10 \times d$ measurement data are required.

6.4.2 Optimizing the Locations of Measurement Data

Since |**M**| is dependent not only on the number of measurement data, but also on the locations of the measurement data, we should also optimize the locations of the measurement data to maximize |**M**|. The parameter variables u and v of the measurement data in the parameter field of the freeform surface constitute the design variables. Each candidate measurement data point can vary its location (u, v) within a specified range. The coordinate (x, y, z) of the measurement data can be obtained from the parameter variables (u, v) by (6.4). Thus, optimizing the locations of the measurement data points for minimizing the uncertainty of a B-spline model can be stated as follows:

$$\max_{u_k, v_k} |\mathbf{M}| \tag{6.13}$$

subject to: $(u_i, v_i) \in [0,1]$, $i=0,1,\ldots m-1$.

The problem is essentially a combinatory optimization problem. Since the objective function |**M**| is non-smooth and nonlinear, the existence of the derivations at all points is not guaranteed. This makes the optimization difficult if a standard optimization method is used. To simplify the problem, |**M**| can be evaluated with an existing discrete D-optimal design method called Fedorov exchange algorithm (Miller and Nguyen 1994). This algorithm implements an efficient neighborhood search for the maximum determinant of the Fisher information matrix **M**.

Consider the incremental form of |**M**|. Each additional measurement data incrementally updates **M**, so that after *i+1* measurements, its value becomes $\mathbf{M}(i+1) = \mathbf{M}(i) + L_{i+1}^T L_{i+1}$. The corresponding determinant of **M** then is

$$| \mathbf{M}(k+1) | = (1 + L_{i+1} \cdot \mathbf{M}^{-1}(k) \cdot L_{i+1}^T) \cdot | \mathbf{M}(k) | \tag{6.14}$$

where $L_{i+1} = [\mathbf{B}_{i+1}, \mathbf{B}_{i+1}, \mathbf{B}_{i+1}]$, $\mathbf{B}_{i+1}$ is the basis function vector evaluated at location (u_{i+1}, v_{i+1}).

If a point is to be removed from the set of sample points, all the plus and minus signs in (6.14) are reversed. To evaluate |**M**| by Fedorov exchange algorithm, each point in the set of measurement data is considered for exchange with each of the available candidate points. The pair of points chosen for exchange is the pair that maximizes the increase in the determinant of **M**. This process is repeated until no further increase in the determinant can be obtained by the exchange.

If we denote the point to be added by L_+, and the point to be replaced by L_-, then by exchanging the pair of L_+ and L_-, the new determinant is

$$| \mathbf{M} + L_+^T L_+ - L_-^T L_- | = | \mathbf{M} | \cdot [1 + \Delta(L_+, L_-)] \tag{6.15}$$

where

$$\Delta(L_+, L_-) = L_+ \mathbf{M}^{-1} L_+^T - L_- \mathbf{M}^{-1} L_-^T (1 + L_+ \mathbf{M}^{-1} L_+^T) + (L_+ \mathbf{M}^{-1} L_-^T)^2 . \tag{6.16}$$

It is obvious from (6.16) and (6.16) that it is critical for the Fedorov exchange algorithm to find a candidate point to replace a point in the current measurement data set in turn, which maximizes $\Delta(L_+, L_-)$. In this work, we used a simulated annealing algorithm to search the candidate point. Simulated annealing (SA) is a random search algorithm that is popular for solving both the continuous and the discrete global optimization problem. The optimal procedure using the discrete SA algorithm for optimization of the locations of the measurement data points can be stated briefly as follows:

- **Step 1** Select a measurement point $r(u_i, v_i) \in S$, $i = 0, 1, \ldots, m-1$ from the set of sample points.
- **Step 2** Generate a candidate point $r_c(u_c, v_c) \in S$ according to a specified generator.

- **Step 3** Set

$$r_i(u_i, v_i) = \begin{cases} r_c(u_c, v_c) & \text{if } \Delta(L_+, L_-) > 0 \\ r_c(u_c, v_c) & \text{with probability } p \text{ if } \Delta(L_+, L_-) < 0 \\ r(u_i, v_i) & \text{otherwise} \end{cases}$$

where p is the probability of accepting p when $\Delta(L_+, L_-)<0$. For simplicity, the probability p is set as constant.

- **Step 4** Repeat Step 2 and 3 until the stopping criterion is satisfied.
- **Step 5** Select another measurement data point from the sample set, and repeat step 1–4 until all measurement data in the selected measurement are exchanged.

6.5 Experiments

To demonstrate the effectiveness of the proposed sensor planning strategy for reconstructing freeform surfaces, experiments are conducted. In the current implementation, a uniform cubic B-spline model is used to represent these surfaces.

One example is an object manufactured in our own laboratory. This object has a freeform surface contained in an area of 40×40 mm^2 and a depth of 10 mm, as shown in Fig. 6.2a.

To reconstruct the freeform surface, the first thing is to determine the control point number n_u and n_v of the B-spline model in the u and v parameter directions. A 3D vision system was used to acquire a cloud of data points on an object surface. This vision system (Kreon/KLS51 by Kreon Technologies) consisting of a laser stripe projector and CCD camera measures 3D coordinates based triangulation. The measurement for the above example object is shown in Fig. 6.2b. We used our Modified BIC criterion to select the B-spline model structure (n_u and n_v) for

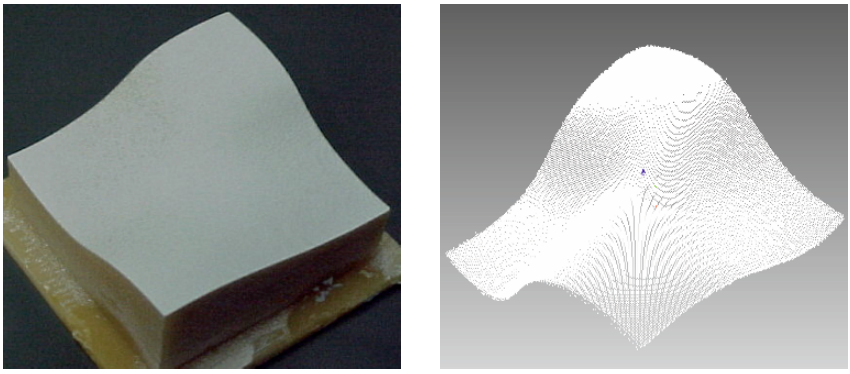

(**a**) The object with a freeform surface (**b**) The point cloud acquired by a 3D vision sensor

Fig. 6.2. The experimental object

representing the freeform surface. To demonstrate the effectiveness of the modified BIC criterion, we compared it with the BIC and cross validation (CV) methods (Cherkassky et al. 1999, Mcquarrie and Tasi 1998) respectively. The two following performance indexes were used:

1. Estimation accuracy, which is defined as the MSE (Mean Square Error) between the actual data points and the regression estimate chosen by a given model selection method;
2. Model complexity, which refers to the number d ($d = n_u \times n_v$) of control points of a B-spline model determined by a given model selection criterion.

In this section, we use box plots of the MSE and model complexity of each method to test the performance of different model selection methods. The experiments with different sample sizes were designed to observe the differences between the different model selection methods. For each sample size, the sample points were selected randomly from the "data cloud" acquired by the 3D vision system, and then used to determine the model structured out of the B-spline model with a different model selection criterion. The above selection process was repeated 100 times. The comparison results are presented in Box plots which give the empirical distribution of the comparison based on 100 iterations in the model selection. An evaluation result with a set of 300 sample points is shown as a box plot in Fig. 6.3. In this figure, the box represents the range of distribution of the quantity under study. The box stretches from the lower hinge (defined as the 25th percentile) to the upper hinge (the 75th percentile) and therefore contains the middle half of the scores in the distribution. The dark line (shown as across a box) is the median of the quantity. Therefore ¼ of the distribution of a box lies between this dark line and the top of the box, and ¼ of the distribution lies between this dark line and the bottom of the box.

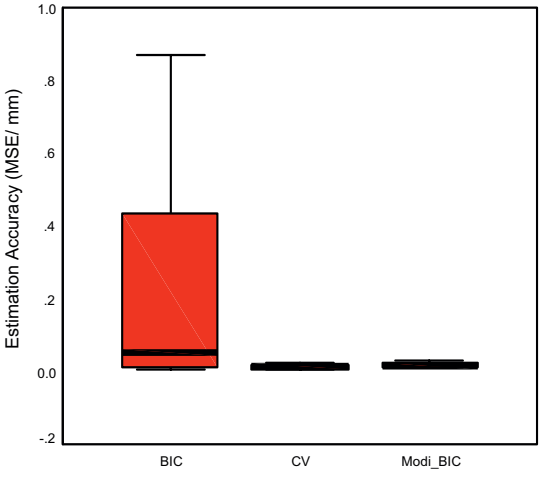

Fig. 6.3. Estimation Accuracy

The MSE box plot, in combination with the box plot of model complexity (i.e. the number of control points), provides visual judgment on the relative performance of various model selection methods. A lower value of MSE in the plot corresponds to a better model selection approach. The model complexity plot, together with the estimation accuracy plot, provides information on the over-fitting or under-fitting for a given method relative to the optimally chosen model complexity. The height of the bar in the plots of the estimation accuracy reflects the method's sensitivity to random sample variations, which can be used as a measure of the variability in the error estimation. A short bar in the plot indicates that the method is insensitive (robust) to random variations in the data. In general, low model complexity is desired. As the number of parameters in a B-spline model is related to its uncertainty, the more the parameters of a B-spline model, the higher the uncertainty tends to be. For a model with high complexity, more measurement data would be needed to increase the reliability in the parameter estimation. In such a case, the time cost in the measurement and reconstruction would be high.

From Figs. 6.3 and 6.4, the model selected by BIC provides a consistent model structure, which is insensitive to random variances in the data. However, the estimation accuracy is rather poor, compared with the CV and our modified BIC method (denoted as Modi_BIC) as can be seen in Fig. 6.3. In fact, in the BIC criterion, only the second term can prevent over-fitting. As a result, BIC is insensitive to over-fitting and a model with high complexity is selected. On the other hand, the re-sampling procedure in CV and our method has the capability of detecting the occurrence of over-fitting and under-fitting in time. Compared with CV, our criterion results in a similar level of estimation accuracy and provides a

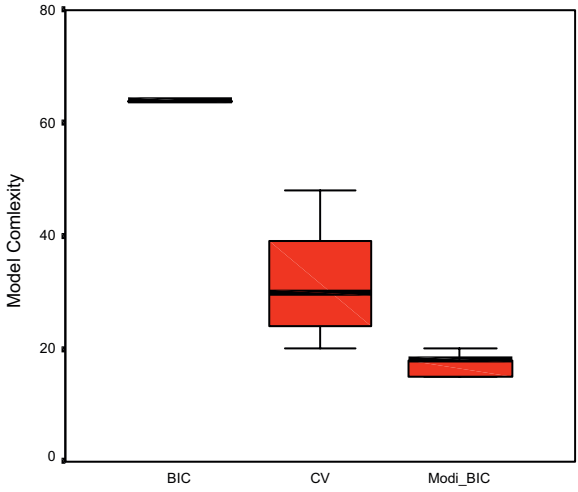

Fig. 6.4. Model complexity (Results with 300 training samples and 200 prediction samples)

lower complexity model with satisfactory consistence. We also compared the performance of the three model selection methods using a larger sample size of 1200. It was observed that the models selected by the three methods had similar levels of estimation accuracy (about 0.012 mm), while the BIC and CV method seem to prefer a model with higher complexity (with the median of 80 for BIC, 69 for CV, and 33 for our modified BIC), although BIC exhibited good consistency and insensitivity to random variances. With our criterion, a much lower model complexity was achieved, while keeping similar estimation accuracy. On the whole, our method achieved a good compromise between the selected model complexity and estimation accuracy.

Then we further tested our method (modified BIC criterion) with different sized samples, where the number of prediction samples used was about 40% of that of the training samples. The results are given in Table 6.1. It can be seen that with the increase in the sample size, the estimation accuracy tends to improve while the model complexity tends to increase. Such an effect becomes less obvious when the sample size is bigger than 1200, where the model complexity and accuracy tend to be stabilized. In such a case, the corresponding model structure can be considered as converged to the true model of the freeform surface. In our system, since we can get a sample set with a sufficiently large size from a cloud of data obtained by the vision system, we can assume that the true model structure to describe the unknown freeform surface can be obtained.

Here, we used bi-cubic B-splines to model the freeform surface. Different B-spline models with different control points in u and v directions were evaluated by our modified BIC criterion. The result was a B-spline model with 6 control points in both u and v directions respectively (totally 36 parameters to be estimated) which had the highest scores of our modified BIC. This model is a result yielded by our method to represent the freeform surface to be reconstructed.

Based on the selected B-spline model, the minimal set of 360 measurement data was used to estimate these parameters. As discussed in Sect. 3, high uncertainty in the estimated parameters indicates that the estimated values of $\hat{\mathbf{\Phi}}$ can deviate significantly from the true values of $\mathbf{\Phi}$. In other words, the lower the uncertainty in the estimated parameters, the more reliable the estimation $\hat{\mathbf{\Phi}}$ is. Here, we use the $\log(|\mathbf{M}|)$ as the indicator of the uncertainty in a B-spline model. The larger the $\log(|\mathbf{M}|)$, the lower the uncertainty.

Table 6.1. Results of model selection by modified BIC with different sample sizes

Sample size	200	300	500	800	1200	1600	2000	2500
Accuracy (MSE)	0.075	0.019	0.022	0.019	0.015	0.015	0.015	0.015
Model Complexity	2×3	4×4	4×4	4×5	6×6	6×6	6×6	6×6

Next, we employed the Fedorov exchange algorithm to optimize the locations of the measurement data. The locations of the measurement data before and after the optimization are shown in Figs. 6.5 and 6.6. Before optimization, the measurement data were located randomly in the parameter space (u, v) of the B-spline surface, with the uncertainty of the B-spline model log(|**M**|) being –120. Using the Fedorov exchange algorithm, the locations of sample points were adjusted one by one, with the log(|**M**|) value of the B-spline model increased gradually to –94.5, which shows a significant decrease in the corresponding uncertainty of the B-spline compared with using random locations in the measurement data. On the other hand, increasing the sample size can also reduce the uncertainty of a B-spline model. To achieve the same level of uncertainty in the B-spline model with random locations in the

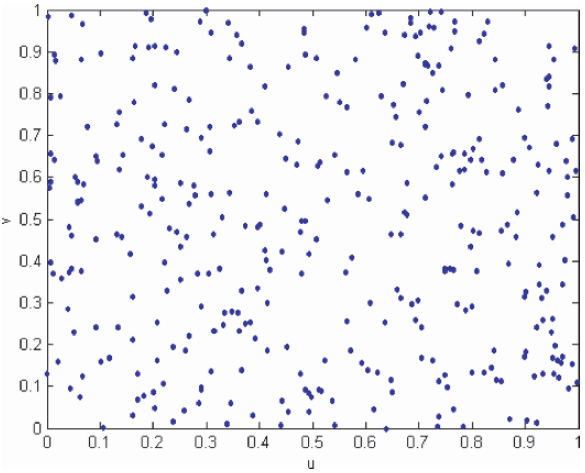

Fig. 6.5. The locations of the measurement data before optimization

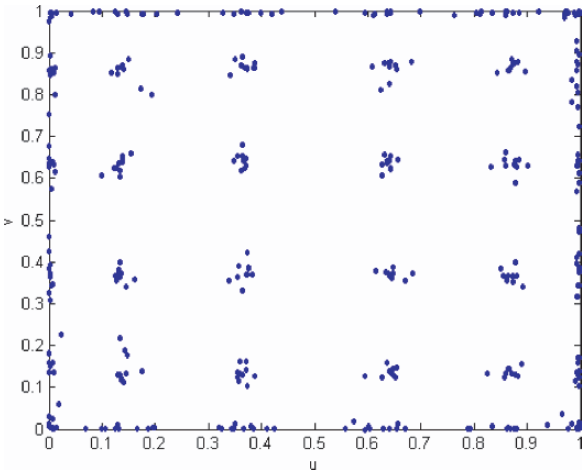

Fig. 6.6. The locations of the measurement data after optimization

measurement data, about 470 more measurement data would be needed in the sample set. This shows that optimizing the locations of the measurement data point to be sensed by CMM's touch probe can yield much more reliable model estimation, without increasing the number of measurements to be taken. We also compared our optimization results with a measurement of equidistant probing points. The uncertainty $\log(|\mathbf{M}|)$ of the B-spline model using equidistant probing was found to be –220.1 which is much worse than our optimization result.

Here an interesting phenomenon to note concerning the optimized locations of the measurement data is that after optimization, the measurement data are located in the neighborhood of each model parameter. These relocations allow for a more reliable model estimation in the parameterization space. The coordinates (x, y, z) of the measurement data can be mapped from the parameter variables (u, v) with appropriate coordinate transformations. Finally, the surface of the object in Fig. 6.2, reconstructed using our method, is shown in Fig. 6.7. Here, the mean deviation of the measured coordinates from the reconstructed surface is 0.012 mm, while the minimum deviation is 0.0011 mm and the maximum deviation is 0.028 mm.

From the experiments, we observed that in the parameter space, the locations of the measurement data points are related to the structure of the B-spline model. For a uniform cubic B-spline model, the control points are distributed uniformly in the u and v directions, giving rise to some clusters in which the measurement data points are located. Therefore, we infer that the structure of a B-spline model determines the locations of the measurements and the model structure represents the geometrical feature of a surface, which can be extracted from the cloud of data acquired by a vision system. In addition, as there is a coordinate transformation

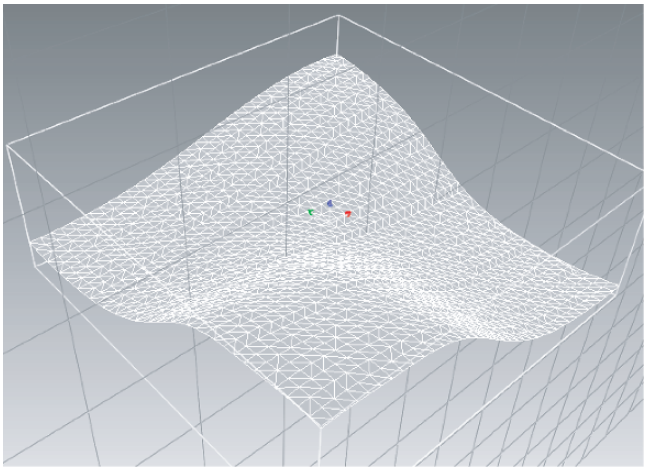

Fig. 6.7. The reconstructed freeform surface

between the location parameters (u, v) and the corresponding spatial coordinates (x, y, z), different parameterization methods can influence the optimization results. We further infer that if we locally modify the distribution of the control points according to the geometrical feature of a surface, the distribution of the measurement data will be changed accordingly.

6.6 Summary

In this chapter, we present a sensing strategy for optimal measurements for the reconstruction of freeform surfaces. We assume the availability of a vision system to quickly obtain the rough data of a surface for guiding the more accurate but much slower touch sensing such as the touch probing in CMM. We investigated the use of B-spline models to represent freeform surfaces and proposed the modified BIC method for selecting the optimal model structure from the cloud of data points acquired by a 3D vision system. Based on the model structure, the number of measurement data needed for the high-precision measurement is then determined. In order to obtain a more accurate model, the uncertainty of the model is analyzed. Then using the statistical analysis of the Fisher information matrix, the locations of the measurement data points are optimized to reduce the uncertainty in the model. Based on the results of the optimized measurements, a more accurate touch sensing, e.g. by CMM's touch probe, can be used to obtain the accurate measurements for the reconstruction of the freeform surface more efficiently. The proposed method will allow the advantages of the high speed in vision sensing and the high accuracy in touch sensing to be utilized for efficient and accurate reconstruction of freeform surfaces. The experimental results show that the proposed method is effective and promises useful applications in integrated multi-sensor measurements such as vision-guided CMM for reverse engineering. When combined with an adaptive modeling scheme based on the features of a freeform surface, adaptive localization of the measurement data points can also be implemented.